ADVANCED ENERGY MATERIALS
www.advenergymat.de

Carbazole Treated Waterproof Perovskite Films with Improved Solar Cell Performance

Jaeki Jeong, Thanyarat Chawanpunyawat, Minjin Kim, Vladislav Sláma, Nikolaos Lempesis, Lorenzo Agosta, Virginia Carnevali, Qihao Zhang, Felix T. Eickemeyer, Lukas Pfeifer, YeonJu Kim, Ji Won Song, Haizhou Lu, Masaud Almalki, Sung-In Mo, Shaik Mohammed Zakeerudin, Ursula Rothlisberger,* Dong Suk Kim,* Paul J. Dyson,* and Michael Grätzel**

Surface passivation has been widely employed to suppress non-radiative charge recombination and prevent interfacial charge accumulation in perovskite photovoltaics. In this report, carbazole modified with ammonium iodide connected via alkyl chains of different lengths (i.e., ethyl, butyl, and hexyl chains) is used to form passivation layers on formamidinium lead triiodide $FAPbI_3$-based perovskite films to improve operational stability. Owing to the strong hydrophobicity of the carbazole moiety, it is observed that the perovskite films with a carbazole passivation layer retain their initial properties even after direct contact with a water droplet for 100 s. In addition, carbazole treatment reduces the rate of trap-assisted recombination at the surface and grain boundaries of the perovskite layer. Furthermore, it accelerates interfacial hole transfer from the perovskite to the charge transport layer. As a result, devices treated with carbazole hexylammonium iodide achieve a power conversion efficiency (PCE) of up to 24.3% during quasi-steady-state (QSS) measurements with extraordinary long-term operational stability under conditions of the ISOS-L-1 protocol, maintaining 95% of their initial efficiency after 1000 h.

1. Introduction

Formamidinium lead iodide ($FAPbI_3$) perovskite has been widely investigated for the preparation of high-efficiency solar cells as its bandgap is close to the Shockley-Queisser (SQ) limit, and it has a longer carrier lifetime and higher phase stability compared to methylammonium A-cation based lead halide perovskites.[1–9] State-of-the-art perovskite solar cells (PSCs) exceeding 25% power conversion efficiency (PCE) have employed $FAPbI_3$-based perovskite materials as the absorber layer.[10–14] However, $FAPbI_3$ perovskite suffers from defects inducing or accelerating the degradation of its crystal structure at the interface between the perovskite and charge transport layers or at grain boundaries (GBs) of the light absorber, inhibiting device performances from approaching their

J. Jeong, T. Chawanpunyawat, F. T. Eickemeyer, L. Pfeifer, H. Lu, M. Almalki, S. M. Zakeerudin, M. Grätzel
Laboratory of Photonics and Interfaces
Institute of Chemical Sciences and Engineering
École Polytechnique Fédérale de Lausanne (EPFL)
Lausanne CH-1015, Switzerland
E-mail: lukas.pfeifer@epfl.ch; michael.graetzel@epfl.ch

J. Jeong, P. J. Dyson
Institute of Chemical Sciences and Engineering
École Polytechnique Fédérale de Lausanne (EPFL)
Lausanne CH-1015, Switzerland
E-mail: paul.dyson@epfl.ch

The ORCID identification number(s) for the author(s) of this article can be found under https://doi.org/10.1002/aenm.202401965

DOI: 10.1002/aenm.202401965

J. Jeong
Department of Energy Science
Sungkyunkwan University
Seoburo, Suwon 2066, Republic of Korea

M. Kim, S.-I. Mo
Ulsan Advanced Energy Technology R&D Center
Korea Institute of Energy Research
25 Techno Saneop-ro 55beon-gil, Nam-gu, Ulsan 44776, Republic of Korea

V. Sláma, N. Lempesis, L. Agosta, V. Carnevali, Q. Zhang, U. Rothlisberger
Laboratory of Computational Chemistry and Biochemistry
École Polytechnique Fédérale de Lausanne (EPFL)
Lausanne CH-1015, Switzerland
E-mail: ursula.roethlisberger@epfl.ch

Y. Kim
Laboratory for Molecular Engineering of Optoelectronic Nanomaterials
Institute of Chemical Sciences and Engineering
École Polytechnique Fédérale de Lausanne (EPFL)
Lausanne CH-1015, Switzerland

theoretical limit.[6,15,16] To overcome this drawback, surface passivation has been widely considered as one of the most effective strategies for suppressing interfacial defects and trap-assisted recombination in treated perovskite films leading to an improvement of the PCE.[17–19] A further advantage of molecular passivators is that they may enhance device stability by preventing the perovskite layer from getting into contact with components from the adjacent hole transport layer (HTM) and moisture or oxygen from the ambient air.[20,21]

Since the first report of surface treatment with phenylethylammonium iodide by Jiang,[17] a wide range of organic ammonium salts containing different backbones have been investigated and employed either in the form of an additive to the perovskite precursor solution or as an interlayer between the perovskite and HTM.[17,22,23] To date, octylammonium iodide (OAI) and bromide (OABr) have become widely used to enhance the performance of PSCs.[24,25] Recently, Tan and co-workers reported that counter-anion engineering with tosylate further improves the stability of FA-based PSCs by decreasing its work function.[26] Additionally, Pitaro et al. employed carbazole derivatives as an amphiphile at the interface between the perovskite and organic HTL layers in an inverted device structures.[27,28] Moreover, different kinds of passivating agents leading to improved photovoltaic performance and enhanced stability have been studied by varying either the organic cation or the counter-anion.[29–32]

Although these passivators can achieve high efficiencies and improve device stability under different aging conditions, the identification of molecules that can protect a perovskite film from moisture in humid air remains a challenge.[33,34] In our previous study, PSCs treated with OAI achieved a 25.4% certified efficiency, however, their long-term operational stability was only moderate, highlighting the fact that $FAPbI_3$ is sensitive to the external stress imposed during operation.[13]

In this work, we present a series of carbazole derivatives modified with ammonium iodide connected via alkyl chains of different length (i.e., ethyl, butyl, and hexyl chains termed CEAI, CBAI, and CHAI, respectively) as surface passivators for $FAPbI_3$ and assess the effect of the alkyl chain length on the efficiency and stability of the PSCs. We find that the carbazole-treated perovskite layers present strongly hydrophobic properties thus retaining their PV performance when exposed to ambient moisture. The hydrophilic ammonium moiety of the carbazole derivative replaces formamidinium on A-cation surface sites forming a self-assembled monolayer, directing the carbazole moiety to the interface where it forms a stable contact with the hydrophobic HTM mitigating the formation of interfacial defects. As a result, we obtained a PCE of 24.3% in quasi-steady state *I-V* measurements, with >83% FF and a high operational stability. Remarkably, an unencapsulated cell retained 95% of its initial efficiency after 1000 h under maximum power point tracking as specified by the ISOS-L-1 test protocol.[35]

2. Results and Discussion

In order to fabricate black α-phase $FAPbI_3$ perovskite film with large grain size, we employed a precursor solution containing black $FAPbI_3$ powder and methylammonium chloride (MACl).[36] CEAI, CBAI, and CHAI were coated on top of the perovskite film (**Figure 1a**, details of their synthesis are provided in the Supplementary Material). The aromatic structure of carbazole helps with charge delocalization augmenting its hydrophobicity.[37] The ammonium group tethered via the alkyl chain serves to anchor the carbazole to the perovskite surface, with the length of the alkyl chain allowing the packing and hydrophobicity of the passivator to be fine-tuned.

To investigate the effect of the passivation layer, scanning electron microscopy (SEM, Figures S2 and S3, Supporting Information) and UV–vis spectroscopy (Figure S4, Supporting Information) measurements were carried out on stacks of bare glass/perovskite/passivation layer. A uniform and pinhole-free crystalline film morphology was observed for both the pristine film, hereafter denoted control, and carbazole-treated perovskite films and the absorption threshold was identical for all films. These results imply that interaction between $FAPbI_3$ and ammonium alkyl iodide has no effect on the absorption spectrum of the perovskite. The energy level diagrams of perovskite films, both with and without a passivation layer, were characterized using ultraviolet photoelectron spectroscopy (UPS), as shown in Figures S5 and S6 (Supporting Information). The valence band offset between CHAI and perovskite (−5.39 eV) creates a driving force of 30 meV for hole transfer from perovskite to CHAI. This results in a favorable band alignment with the perovskite, potentially minimizing the voltage loss in the resulting device. Next, the contact angles of water droplets deposited onto control and films passivated with CEAI, CBAI, and CHAI were measured. Figure 1b shows that the contact angles dramatically increase up to 81.5° (54.3° for control) for carbazole-treated perovskite films, indicative of a strongly hydrophobic layer on the perovskite surface. These values are superior to those of the widely used ammonium salts, such as OAI (66.15°) and PEAI (62°), showing that the carbazole-containing agents may be apt to inhibit phase degradation in a humid atmosphere.[20,38] To verify the formation of monolayers by carbazole derivatives, we measured the contact angles formed at the perovskite surface with a Spiro-OMeTAD solution in chlorobenzene: Data are shown in Figure S7 (Supporting Information). Notably, there was no difference in contact angles between films prepared using spin-coating and dip-coating methods. This consistency indicates that the carbazole layer is indeed forming a monolayer.[39]

The stability of the passivated perovskite films toward moisture was tested under continuously controlled aging conditions, in which a closed box filled with air was used with a relative humidity (RH) of 99%. Degradation of the perovskite films was monitored by taking photos over time (Figure S8, Supporting Information). Control and OAI-treated perovskite films started to degrade after only 2 days of aging whereas the carbazole-treated perovskite films retained their initial appearance for 30 days. In addition, the structural stability of the passivated perovskite films

J. W. Song, D. S. Kim
School of Energy and Chemical Engineering
Ulsan National Institute of Science and Technology (UNIST)
Ulsan 44919, Republic of Korea
E-mail: kimds@unist.ac.kr
M. Grätzel
SKKU Institute of Energy Science and Technology (SIEST)
Sungkyunkwan University
Suwon Republic of Korea

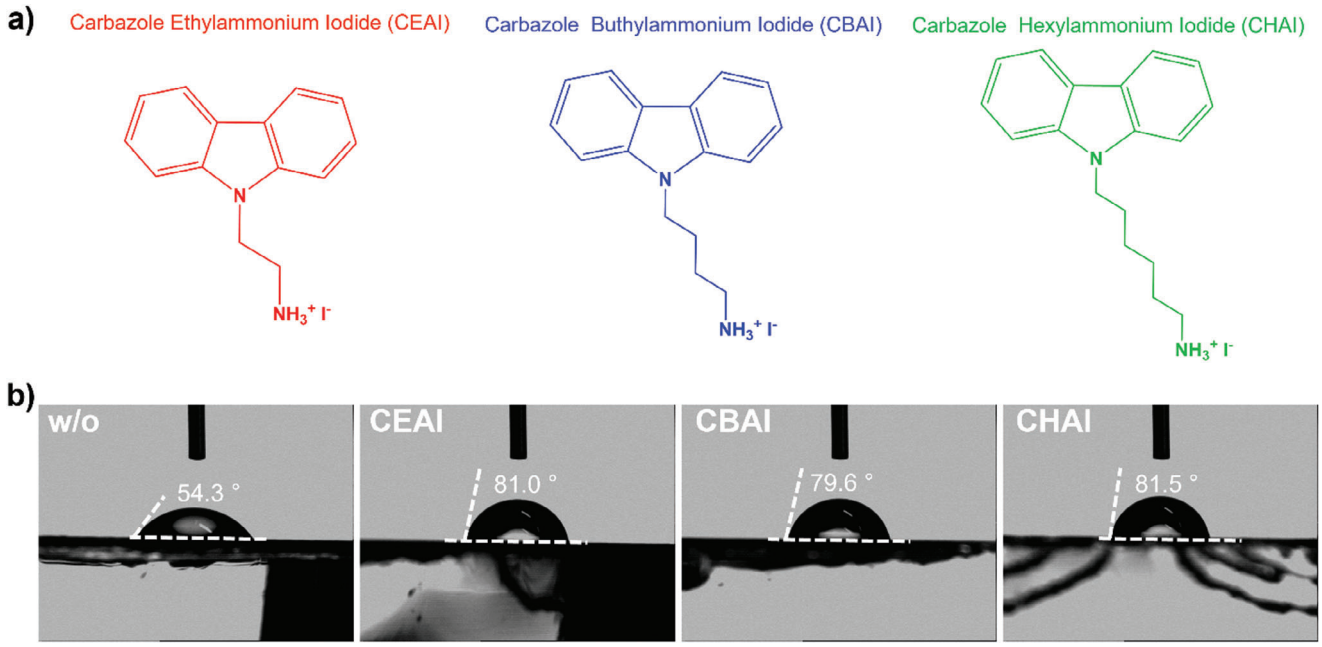

Figure 1. a) Structures of the carbazole alkyl ammonium iodide compounds. b) Contact angle of control and perovskite films treated with CEAI, CBAI, and CHAI, respectively.

was tested by dynamically applying 100 µL of deionized water during spin-coating to determine the extent to which the carbazole-treated perovskite films retained their hydrophobic properties under centrifugal force. Interestingly, **Figure 2**a shows that the control and reference (OAI) films completely transform into yellow PbI_2. In contrast, the film treated with CHAI preserved its black phase α-$FAPbI_3$ structure during spin-coating. X-ray diffraction (XRD) measurements confirmed these observations. As shown in Figure 2b, there was no significant difference regarding the position of the XRD peaks for the carbazole-treated films before and after water dripping under centripetal force. Encouraged by these results, a water droplet was deposited on top of different perovskite films. Figure 2c shows that both the control and OAI-treated film were destroyed within only 5 s, whereas the film with CHAI maintained a black α-$FAPbI_3$ perovskite layer for ≈90 s. Consequently, the strongly hydrophobic surfaces generated with our carbazole amphiphiles effectively attenuate moisture-induced degradation.

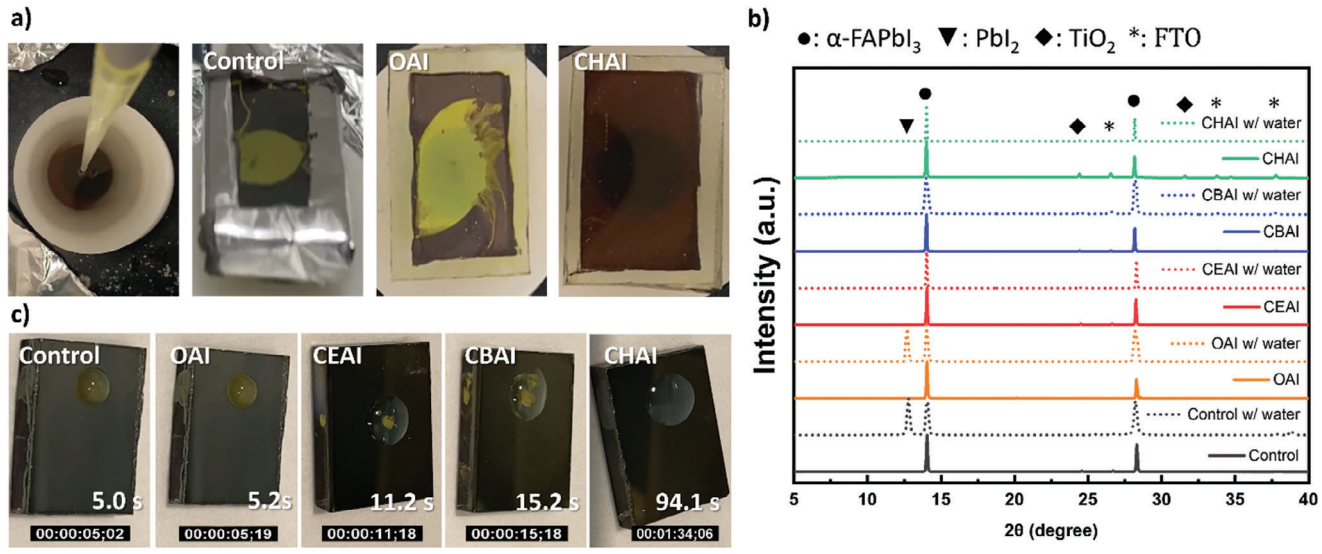

Figure 2. a) Photographs of the control film and films with OAI (reference film) and CHAI passivation layers after dynamically applying a 100 µl drop of deionized water during spin-coating. b) Corresponding XRD diffraction spectra before and after treatment with water. c) Photographs of the control film and films with OAI (reference film) CEAI, CBAI, and CHAI passivation layers recorded at the given time point after statically applying a 100 µl drop of deionized water, marking the onset of visible film degradation.

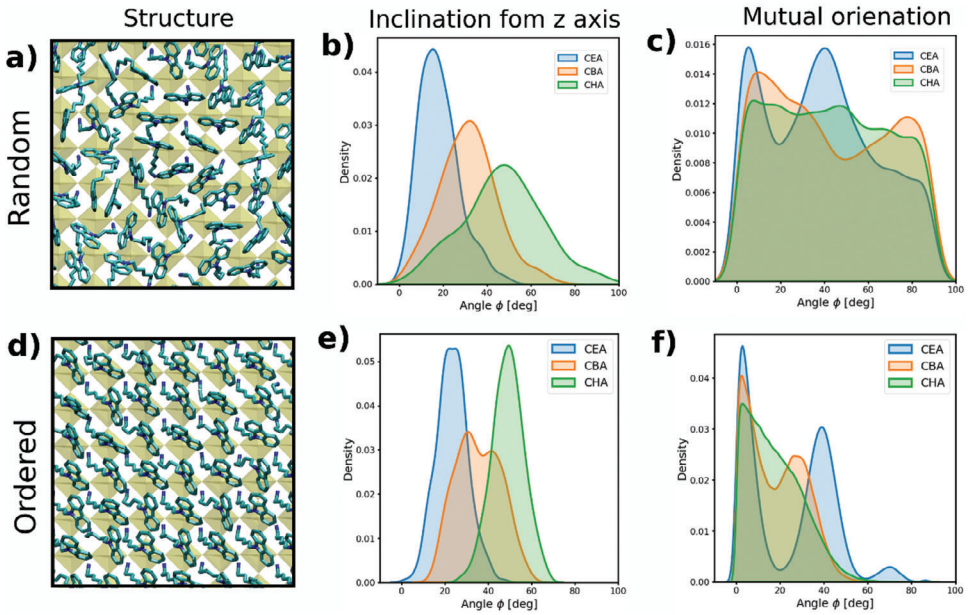

Figure 3. Molecular stacking of carbazole-treated surfaces. a–c) correspond to the randomly self-assembled surfaces, whereas d–f) refer to the ordered ones. The z-axis is defined as perpendicular to the perovskite surface. Parts (b) and (e) show histograms of the inclination angle of the longitudinal axis of the carbazole compounds (red vector in Figure S10, Supporting Information) away from the z-axis, whereas parts (c) and (f) show histograms of the angle formed between the planes of the rings of neighboring carbazole compounds (blue vector in Figure S10, Supporting Information) corresponding to their mutual orientation during self-assembly.

2.1. Molecular Mechanism of Carbazole Passivation

The stability and structure of the absorbed layer are largely influenced by the binding energy of the carbazole alkyl ammonium chain to the surface. A larger binding energy leads to a more stable passivation layer and a higher probability for uniform coverage of the surface. The binding energies of PEA^+, OA^+, and the different carbazoles additives, with respect to the binding energy of FA, were computed at the quantum mechanical level (see Supplementary Materials). The ordering of individual cations from the weakest binding to the strongest is as follows: FA+ < OA+ < PEA+ < CEA+ < CBA+ < CHA+. The relative energies together with the discussion of different approaches for computing binding energies are present in the Supplementary Materials. All investigated additives exhibit stronger binding energies than FA+, suggesting stable binding of the additives to the perovskite surface and preferred surface substitution of FA+ favoring uniform coverage of the surface. Moreover, the binding strength increases with increasing length of the alkyl chain leading to the most stable surfaces being formed by CHAI. The weaker adsorption of PEA+ with respect to carbazoles is also in line with the higher stability of carbazole additives. The increase in binding energy with longer alkyl chain length can be related to the growing amount of dispersion interaction which accounts for >50% of the binding energy difference from FA+ (see Supplementary Materials). Stronger binding reduces the probability of defect formation, which is in line with the experimental results, where the best surface protection was observed for CHAI. The larger binding energy of the CHA+ with respect to FA+ also leads to strong stabilization of the surface. This results in passivated surface, which is more stable than the FAPbI3 bulk. In fact, the surface energy for the optimized structures of the CHAI passivated surface is EsurfCHA = −0.26 eV nm^2 whereas for the pure FA-terminated surface it is significantly larger EsurfFA = 1.69 eV nm^2 (negative values represent surface stabilization while positive ones imply an energetically less favorable surface than the bulk). The calculated surface stabilization by CHAI corresponds to the perfectly ordered, periodic, and non-defective system.

One of the most crucial factors influencing the effect of the carbazole additives is the structure of the adsorbed layer. In the absence of atomically resolved structures, we investigated two different scenarios involving a disordered and an ordered monolayer, respectively. Both systems comprised a 16 × 16 × 4 $FAPbI_3$ supercell and a total of 256 carbazole compounds for perfect monomolecular coverage. The first (disordered) set was created by self-assembly of the carbazole molecules initially scattered randomly above the $FAPbI_3$ surface utilizing classical Molecular Dynamics (MD) simulations (**Figure 3a**). The second set corresponded to a perfectly ordered stacking of the carbazole molecules along the surface (Figure 3d). The initial conformation of the carbazole molecules for the ordered surfaces was obtained from structural analysis of the randomly self-assembled surfaces, where smaller areas of highly ordered adsorbed molecules were observed. All the surfaces were carefully equilibrated first by simulated annealing at 400 K and subsequently cooling to 300 K for 10 ns. For the uniform monolayer coverage of the surface, both ordered, and randomly assembled surfaces show an upright orientation of the adsorbed carbazole molecules with respect to the perovskite surface (Figure S9, Supporting Information). With increasing length of the alkyl chain, tilting of the carbazole ring system toward the surface, defined by the vertical inclination of the shorter symmetry axis of the carbazole head group (Figure S10,

Table 1. Summary of the most important structural parameters obtained from the molecular simulations of the surfaces treated with different carbazole compounds. Water penetration is defined as the fraction of water molecules found inside the perovskite layer.

	Random			Ordered		
	CEA^+	CBA^+	CHA^+	CEA^+	CBA^+	CHA^+
Water penetration	10.3%	6.4%	6.0%	4.0%	3.5%	0.0%
Contact angle [deg]	57.2 ± 0.8	67.8 ± 0.8	72.0 ± 0.7	77.4 ± 0.7	79.2 ± 0.7	81.1 ± 0.6

Supporting Information), increased from 18° for CEA^+, to 48° for CHA^+ (Figure 3b,d). For the tilted molecules, the carbazole heads come into close contact thereby providing enhanced surface coverage (88% for the ordered layer of $CHAI^+$ against 72% for its random counterpart, Figure S11, Supporting Information). Furthermore, the mutual intermolecular orientation of the carbazole molecules on the surface is significantly different between ordered and randomly oriented surface layers (Figure 3c,d). For the randomly assembled case we observed almost no preferential ordering of the carbazole compounds except for CEA^+ where larger ordered areas were observed. On the other hand, the ordered structures remained close to the initial conformations even at room temperature. This is because the bulky carbazole head restrains the free rotation of single molecules due to steric interactions with neighboring molecules. Therefore, only collective motions involving several carbazole molecules on the surface would lead to considerable conformational changes within the ordered layers.

The stability of the ordered and randomly self-assembled surfaces was compared for the optimized structures of the CHAI treated systems at the classical (force field) level. The ordered structure is energetically more favorable by 1.2 kcal per surface unit cell.

Hydrophobicity and associated protection against humidity were investigated by adding a water droplet of 4.5 nm diameter (1590 water molecules) on top of the equilibrated carbazole-treated surfaces, as well as on the untreated perovskite surface (control). For all treated surfaces, MD simulations revealed increased hydrophobicity and significant protection against water penetration compared to the untreated control surface (Figure S12, Supporting Information). For the untreated surface, water readily spreads out over the surface leading to fast degradation of the perovskite. Interestingly, the average calculated contact angles differ largely when comparing random to ordered stacking arrangements with the ordered packing yielding values in remarkable agreement with our experiments (**Table 1**; Figure S13, Supporting Information) strongly suggesting that all three carbazole derivatives indeed form highly ordered self-assembled monolayers. In parallel, the simulations show that the amount of water penetrating through the organic layer into the perovskite decreases with the level of carbazole surface organization and the length of the carbazole alkyl chain dropping from 10.3% water penetration for the random CEAI layer to a striking 0% for the ordered CHAI layer (Table 1). Compared to the simulation of the OAI-treated surface, exhibiting 51.3% water penetration, all studied carbazole surfaces provided exceptional protection against moisture. PEAI provides much better protection against moisture than OAI, however, with 13.1% of water penetration to the surface, its performance is still worse than all studied carbazole-based additives. The low water protection ability of OAI was associated with its highly mobile alkyl chain,[40] which offers more space for water incursion toward the surface compared to the bulkier and less flexible carbazole heads. Similarly, PEAI, for which the phenyl group is still smaller than the carbazole head group, leaves more surface exposed to the water molecules. On the other hand, the phenylethyl tail mobility is significantly reduced compared to the alkyl chain of OAI, leading to somewhat enhanced surface protection. Apart from the more pronounced hydrophobic character, enhanced moisture protection is attributed to the molecular tilting of our carbazole additives leading to a maximum of 88% surface coverage for the ordered CHAI layer (Figure 3; Figure S11, Supporting Information). In general, the ordered surfaces provide far better protection than the randomly assembled ones (Table 1 and **Figure 4**) which can be explained by the restricted motion of the individual carbazole heads and the persistent close packing yielding an efficient surface screening against moisture. On the other hand, in the randomly assembled surfaces thermal fluctuations can dynamically create small openings in the adsorbed layer, allowing water molecules to penetrate the perovskite. In line with the water penetration results, the randomly assembled surfaces showed smaller contact angles and therefore lower hydrophobicity compared to the ordered ones (Figure S13, Supporting Information). As an extra point of comparison, we calculated the water diffusion coefficient, *D*, in all three directions for a system comprising a 1.5 nm thick water layer on top of the perfectly ordered carbazole-treated surfaces. The diffusivity of water in the z-direction, i.e., normal to the treated surface, is hampered by the presence of the carbazole layer. Interestingly, the reduction of water diffusivity normal to the surface is more pronounced for the CHAI-treated surface further validating the water-repelling character imparted to the perovskite surface through CHAI treatment (Figure S14, Supporting Information). Correspondingly, the diffusion coefficients in the in-plane directions, x and y, show a subtle enhancement with increasing alkyl chain length because of the stronger repulsion in the out-of-plane z-direction (Figure S14 and Table S3, Supporting Information). From the set of computationally investigated carbazole compounds, CHA^+ shows the best protection ability in terms of binding energy, water penetration, wetting contact angle and hampered water diffusion, which agrees well with the experimental observations.

In addition to the simulations of complete monolayer coverage of the perovskite surface by carbazole molecules, we performed simulations considering carbazole compounds in excess and in deficit. However, neither of these scenarios yielded stable water droplets on the treated surface (Figure S15, Supporting Information). Hence, we conclude that all investigated

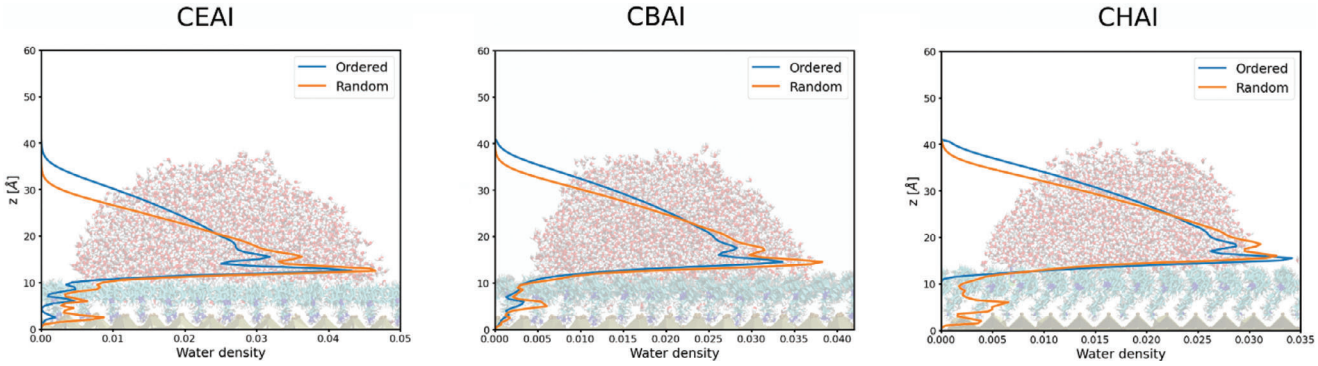

Figure 4. Probability distributions for observing water molecules at a certain height off the perovskite surface for the randomly assembled and ordered surfaces treated with different carbazole molecules. For each distribution the shape of the water droplet extracted from the MD simulation of the ordered surface is included. The origin of the z coordinate is aligned with the top Pb layer of the perovskite.

carbazole additives are likely adsorbed on the surface as uniform monolayers.

2.2. Photovoltaic Performance of the PSCs

The photovoltaic performance of the PSCs containing the control and passivated perovskite films was explored with a configuration comprising FTO/c-TiO_2/SnO_2/perovskite/passivation layer/Spiro-OMeTAD/Au as shown in **Figure** 5a. Quasi-steady-state current-voltage (QSS-IV) measurements were also employed for device characterization to determine accurate device efficiencies with detailed parameters given in Table S1 and Figure S16 (Supporting Information). The device without passivation had a PCE of 21.8% and the device with OAI reached a PCE of 25.2%, with a short-circuit current (J_{SC}) of 26.01 mAcm^{-2}, an open-circuit voltage (V_{OC}) of 1.19, and a fill factor (FF) of 81.41%, consistent with our previous report.[13] Compared with the non-passivated cell, the devices passivated with CEAI, CBAI, and CHAI reached improved PCEs of up to 22.9, 23.7, and 24.8%, respectively. Statistical analysis across 10 devices shows that the improvement compared to the control mainly stems from an increase in V_{OC} and FF (Figure S17, Supporting Information). External quantum efficiency (EQE) measurements were performed to verify the J_{SC} values (Figure 5b). The EQE spectra shows that the integrated J_{SC} values are well matched with the respective results from the QSS-IV measurements. The device with OAI reached a slightly higher integrated current density of 25.6 mAcm^{-2} compared to 25.2 mAcm^{-2} for CHAI. A stabilized PCE of a CHAI-treated PSC of 24.3% was measured under maximum power point

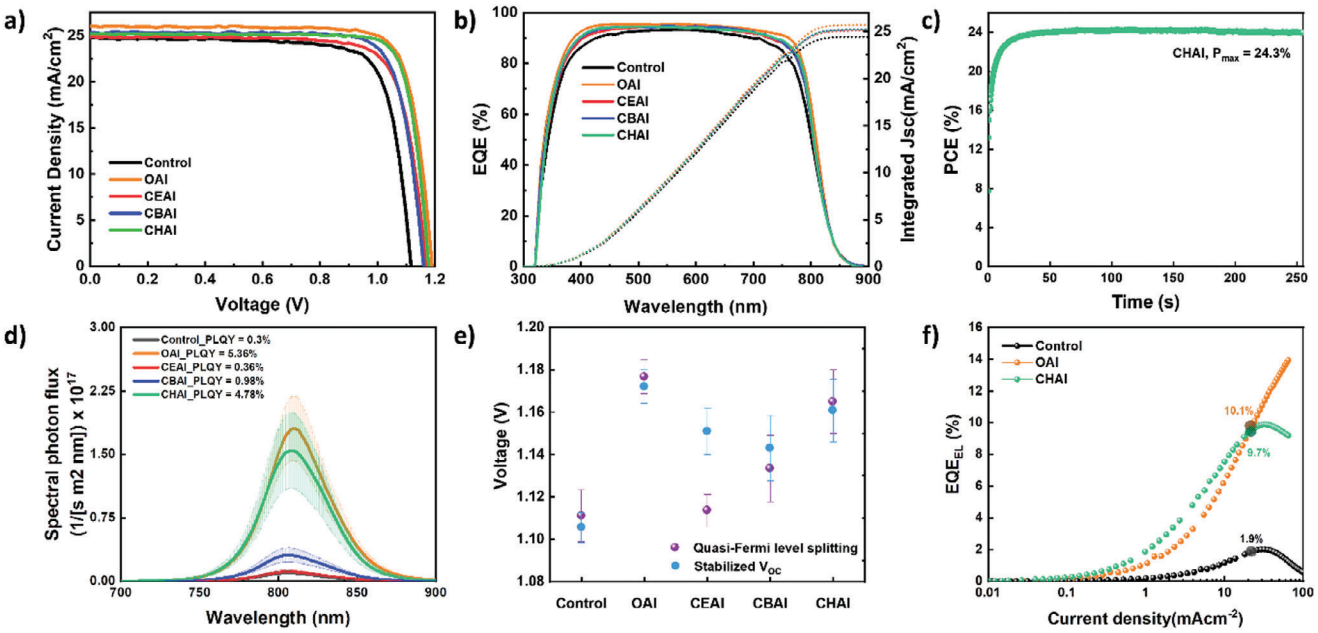

Figure 5. a) *I–V* characteristic of PSCs without and with OAI, CEAI, CBAI and CHAI passivation layers. b) EQE of the PSCs (integrated current densities for the control: 24.45 mAcm^{-2}, OAI: 25.7 mAcm^{-2}, CEAI: 25.1 mAcm^{-2}, CBAI: 25.2 mAcm^{-2}, CHAI: 25.2 mAcm^{-2}). c) The stabilized PCE output of the CHAI-treated champion PSC. d) Absolute photoluminescence intensity and PLQY of perovskite devices and e) stabilized V_{OC} and quasi-fermi level splitting $\Delta E_F/q$ for the layer structure of glass/FTO/SnO_2@c-TiO_2/perovskite/interface layer/HTL. f) EQE_{EL} results of the PSCs.

(MPP) tracking over a period of 250 s (Figure 5c; Figure S18, Supporting Information). Apart from improved hydrophobic protection provided by the interlayer, the devices treated with the carbazoles showed competitive device performances compared to OAI-treated devices, implying that the carbazole interlayer not only improves resistance against moisture, but also effectively reduces the rate of non-radiative recombination losses.

To determine the origin of the enhanced efficiencies of the PSCs treated with carbazoles, the time-resolved photoluminescence (TRPL) decays and steady-state PL quantum yields (PLQY) of the films were studied. As shown in Figure S19 (Supporting Information), the perovskite film treated with CHAI presented the slowest PL decay compared to the other films, indicating the lowest density of trap states and largely suppressed non-radiative recombination as a consequence of carbazole treatment.[10,41] Consistent with the TRPL data, a pronounced increase of the PL intensity was observed at a wavelength ≈805 nm. The PLQY values on the glass substrates increase from 10.7% for the control to 22.8% for the CHAI treated perovskite films, underlining the strong effect of defect elimination by surface treatment (Figure S20, Supporting Information). In addition, the devices treated with CHAI exhibited a PLQY of 4.8%, which is more than ten times higher than that of the control cell, confirming that CHAI suppresses non-radiative charge carrier recombination losses.(Figure 5d) The quasi-Fermi level splitting (ΔE_F) was calculated using the equation: $\Delta E_F = qV_{OC,rad} + kT\ln(PLQY)$, where $V_{OC,rad}$ is the radiative limit of V_{OC}. $\Delta E_F/q$ for the films without and with interface layer, data is shown in Figure 5e and Table S2 (Supporting Information). Compared to the control film, the OAI-treated film showed the highest ΔE_F increase of 66 mV while that of CEAI, CBAI and CHAI-treated films increased by 3, 22, and 54 mV, respectively, confirming that passivation prevents interfacial charge carrier recombination. Furthermore, electroluminescence EQE (EQE_{EL}) measurements were carried out on the control and CHAI-treated devices.[42] Figure 5e shows an EQE_{EL} of 9.7% for the CHAI-treated device whereas the control device had an EQE_{EL} of 1.9% at an injection current density of 26 $mAcm^{-2}$, corresponding to J_{SC} under 1-sun irradiation. Therefore, there is about a fivefold improvement, suggesting a significant reduction of non-radiative recombination losses. TRPL, PLQY, and EQE_{EL} measurements all indicate substantial passivation of the defects on the perovskite surface following carbazole post-treatment.

To explore possible interference effects between the passivator and the hole transporter, we performed ab-initio molecular dynamics (AIMD) simulations to probe the interactions between the CHAI-passivated surface and Spiro-OMeTAD (Supporting Movie S1, Supporting Information). The AIMD revealed only weak noncovalent van der Waals interactions between the CHAI layer and Spiro-OMeTAD, and no specific preferred interaction was found. The noncovalent character of the interactions was evidenced by the distribution of the electron density and its gradient as visualized by the NCI-PLOT in Figure S21a,b and Movies S2 and S3 (Supporting Information).[43] Notably, the presence of Spiro-OMeTAD at the interface does not affect the ordering and surface coverage of the carbazole passivating layer (Figure S21c,d, Supporting Information).

2.3. Storage and Operational Stability of PSCs

To evaluate the influence of the carbazole interlayers on photovoltaic stability, the PSC shelf life based on the ISOS-D-1 protocol was determined by storing the unencapsulated devices in the dark at 25 °C with 30–60% RH. **Figure 6b** shows that the PCE of the control cell decreased by ≈40% after aging for 1200 h, whereas the device passivated with CHAI retained an impressive 92% of its initial efficiency after 2000 h, indicating that CHAI-treated devices are more resistant to moisture and oxygen compared to devices without a passivation layer. This finding is in line with the increased surface hydrophobicity of CHAI-treated devices compared to control cells (vide supra). We further monitored the operational stability of a set of PSCs at 25 °C under ISOS-L-1 protocol conditions by aging the unencapsulated devices in a nitrogen-filled environment using MPP tracking at constant 1-sun illumination. As shown in Figure 6a the PCE of the control device dropped to ≈80% compared to its initial value after 490 h of aging. In contrast, the CHAI-passivated device retained 95% of its original PCE after 1000 h. More details can be found in Figure S22 (Supporting Information). From these results, we infer that the use of CHAI as spacer layer between the perovskite and the HTM improves the performance of PSCs by passivating defects acting as charge carrier recombination centers.

To better understand the mechanism behind this improved stability, fresh and aged devices were compared after illumination. It is known that both iodide migration into the HTM and lithium-ion migration into the perovskite lead to a decline in fill factor under operational conditions.[44] Time-of-flight secondary ion mass spectrometry (TOF-SIMS) depth profiles of fresh and aged devices treated with OAI and CHAI were recorded to determine the ion distributions across the interface between the HTM and perovskite layers as shown in Figure 6c. In the case of OAI, the aged device had a higher Li^+ ions intensity across the entire $FAPbI_3$ perovskite film as well as an elevated I^- intensity around the interface compared to the fresh device. In contrast, the aged device with CHAI had a similar I^- distribution as the fresh device and a substantially lower Li^+ intensity compared to the aged device treated with OAI. This difference indicates that CHAI inhibits the migration of Li^+ ions by forming a compact and contiguous monolayer at the interface between the hole conductor and the perovskite, effectively reducing interfacial ion migration.

3. Conclusion

We have demonstrated the role of carbazole passivation agents in improving moisture resistance and long-term stability of $FAPbI_3$-based PSCs. Superior performances were obtained as the length of the alkyl chain linking the hydrophobic carbazole moiety to the ammonium group (which anchors the compound to the perovskite surface) increased, with CHAI-treated films displaying an impressive stability when a water droplet is placed directly onto the film during spin coating. Molecular dynamics simulations showed that the improved moisture resistance can be attributed to the fact that the carbazole derivatives form a highly ordered uniform waterproof monolayer with CHAI exhibiting the most pronounced effect. As a result, carbazole-treated PSCs not only achieved excellent PCEs of up to 24.3% in QSS-IV measurements, but also retained over 95% of their initial efficiency after

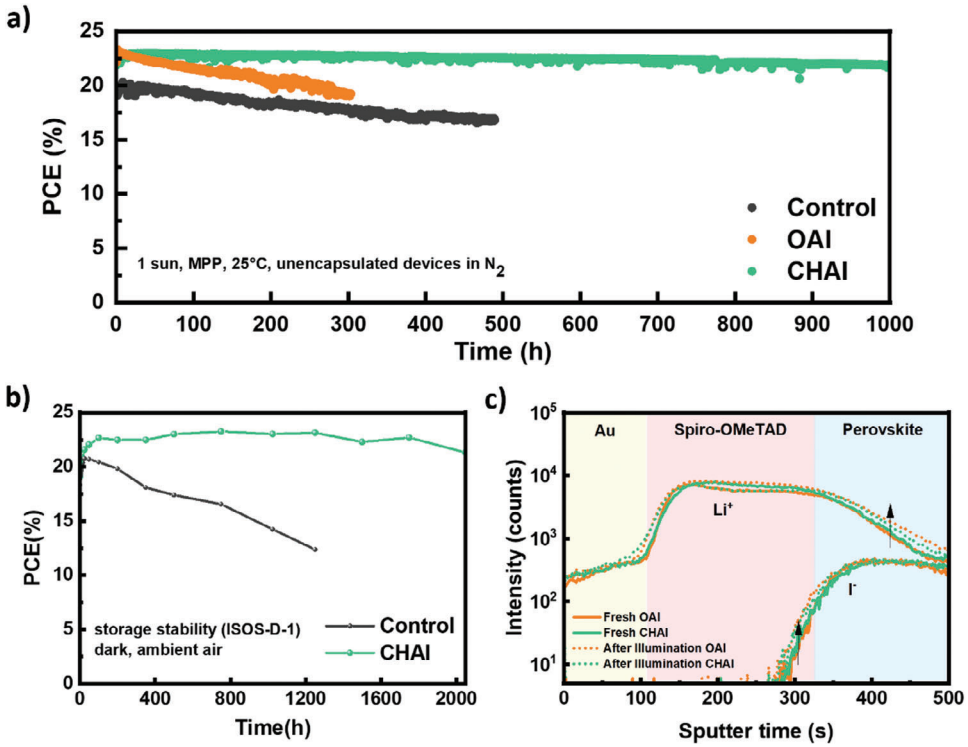

Figure 6. a) Operational stability tests of PSCs at 25 °C under a N_2 atmosphere according to the ISOS-L-1 protocol. b) Shelf-life test (ISOS-D-1) of PSCs in the dark with 30–60% RH. c) TOF-SIMS depth profiles of the fresh and aged devices treated with OAI and CHAI passivation layers, respectively.

aging for 1000 h using MPP tracking under continuous 1-sun irradiation.

Supporting Information

Supporting Information is available from the Wiley Online Library or from the author.

Acknowledgements

The authors thank UNIST Central Research Facilities (UCRF) for the use of its facilities and equipment. This study was funded by the European Union's Horizon 2020 research and innovation program under grant 881603 and a postdoctoral fellowship granted by the National Research Foundation of Korea (NRF, 2021R1A6A3A03039296) and the Swiss National Science Foundation under grant No. 20020–185092. U.R. gratefully acknowledges the Swiss National Foundation (grant N. 200020_219440) and computational resources from the Swiss National Computing Centre CSCS (projects s1151 and s1253). D.S.K. acknowledges the Technology Development Program to Solve Climate Changes of the National Research Foundation (NRF) funded by the Ministry of Science, ICT & Future Planning (NRF-2020M1A2A2080748 and NRF-2023R1A2C3007358). M.A. gratefully acknowledges King Abdulaziz City for Science and Technology (KACST) for the fellowship.

Open access funding provided by Ecole Polytechnique Federale de Lausanne.

Conflict of Interest

The authors declare no conflict of interest.

Author Contributions

J.J., T.C., M.K., and V.S. contributed equally to this work. U.R., D.S.K., P.J.D., and M.G. designed and supervised the project. F.T.E, L.P., and S.M.Z. advised on the research. T.C. and L.P. synthesized organic materials. J.J., T.C., and M.K. developed the concept and analyzed experimental data. Y.K. measured contact angles and XRD spectra. H.L. and F.T.E. performed the EQE_{EL} and PLQY measurements. M.A., J.W.S., Y.J., S.-I.M., and J.-H.O. characterized the perovskite film with UV–vis absorption, AFM, SEM, TOF-SIMS, and TRPL. V.S., N.L., L.A., V.C., and Q.Z. performed the computational work under the guidance of U.R. J.J. wrote the manuscript. M.G., P.J.D., F.T.E., L.P., and U.R. revised the manuscript. All the authors contributed to the discussion of the manuscript.

Data Availability Statement

The data that support the findings of this study are available from the corresponding author upon reasonable request.

Keywords

carbazole derivatives, hydrophobicity, perovskite solar cells, stability

Received: May 4, 2024
Published online:

[1] A. Kojima, K. Teshima, Y. Shirai, T. Miyasaka, *J. Am. Chem. Soc.* **2009**, *131*, 6050.
[2] M. Grätzel, *Nat. Mater.* **2014**, *13*, 838.

[3] J.-P. Correa-Baena, M. Saliba, T. Buonassisi, M. Grätzel, A. Abate, W. Tress, A. Hagfeldt, *Science* **2017**, *358*, 739.
[4] S. Rühle, *Sol. Energy* **2016**, *130*, 139.
[5] Q. Dong, Y. Fang, Y. Shao, P. Mulligan, J. Qiu, L. Cao, J. Huang, *Science* **2015**, *347*, 967.
[6] T. M. Koh, K. Fu, Y. Fang, S. Chen, T. C. Sum, N. Mathews, S. G. Mhaisalkar, P. P. Boix, T. Baikie, *J. Phys. Chem. C* **2014**, *118*, 16458.
[7] Y. Zhang, Z. Zhou, F. Ji, Z. Li, G. Cui, P. Gao, E. Oveisi, M. K. Nazeeruddin, S. Pang, *Adv. Mater.* **2018**, *30*, 1707143.
[8] S. Sánchez, S. Cacovich, G. Vidon, J.-F. Guillemoles, F. Eickemeyer, S. M. Zakeeruddin, J. E. K. Schawe, J. F. Löffler, C. Cayron, P. Schouwink, M. Grätzel, *Energy Environ. Sci.* **2022**, *15*, 3862.
[9] H. Lu, Y. Liu, P. Ahlawat, W. Tress, F. T. Eickemeyer, Y. Yang, F. Fu, Z. Wang, C. Avalos, B. I. Carlsen, A. Agarwalla, X. Zhang, Y. Zhan, S. M. Zakeeruddin, L. Emsley, U. Rothlisberger, L. Zheng, A. Hagfeldt, M. Grätzel, *Science* **2020**, *370*, 6512.
[10] J. Jeong, M. Kim, J. Seo, H. Lu, P. Ahlawat, A. Mishra, Y. Yang, M. A. Hope, F. T. Eickemeyer, M. Kim, Y. J. Yoon, I. W. Choi, B. P. Darwich, S. J. Choi, Y. Jo, J. H. Lee, B. Walker, S. M. Zakeeruddin, L. Emsley, U. Rothlisberger, A. Hagfeldt, D. S. Kim, M. Grätzel, J. Y. Kim, *Nature* **2021**, *592*, 381.
[11] H. Min, D. Y. Lee, J. Kim, G. Kim, K. S. Lee, J. Kim, M. J. Paik, Y. K. Kim, K. S. Kim, M. G. Kim, T. J. Shin, S. Il Seok, *Nature* **2021**, *598*, 444.
[12] Y. Zhao, F. Ma, S. Yu, T. Shen, H.-X. Deng, X. Chu, X. Peng, Y. Yuan, X. Zhang, J. You, *Science* **2022**, *377*, 6605.
[13] M. Kim, J. Jeong, H. Lu, T. K. Lee, F. T. Eickemeyer, Y. Liu, I. W. Choi, S. J. Choi, Y. Jo, H.-B. Kim, S.-I. Mo, Y.-K. Kim, H. Lee, S. Cho, W. Tress, S. M. Zakeerudin, A. Hagfeldt, J. Y. Kim, M. Grätzel, D. S. Kim, *Science* **2022**, *375*, 6578.
[14] J. Park, J. Kim, H.-S. Yun, M. J. Paik, E. Noh, H. J. Mun, M. G. Kim, T. J. Shin, S. I. Seok, *Nature* **2023**, *616*, 724.
[15] Y. Fu, T. Wu, J. Wang, J. Zhai, M. J. Shearer, Y. Zhao, R. J. Hamers, E. Kan, K. Deng, X.-Y. Zhu, S. Jin, *Nano Lett.* **2017**, *17*, 4405.
[16] X. Zheng, C. Wu, S. K. Jha, Z. Li, K. Zhu, S. Priya, *ACS Energy Lett.* **2016**, *1*, 1014.
[17] Q. Jiang, Y. Zhao, X. Zhang, X. Yang, Y. Chen, Z. Chu, Q. Ye, X. Li, Z. Yin, J. You, *Nat. Photonics* **2019**, *13*, 460.
[18] S. Akin, N. Arora, S. M. Zakeeruddin, M. Grätzel, R. H. Friend, M. I. Dar, *Adv. Energy Mater.* **2020**, *10*, 1903090.
[19] E. Aydin, M. De Bastiani, S. De Wolf, *Adv. Mater.* **2019**, *31*, 1900428.
[20] H. Kim, S.-U. Lee, D. Y. Lee, M. J. Paik, H. Na, J. Lee, S. I. Seok, *Adv. Energy Mater.* **2019**, *9*, 1902740.
[21] A. R. bin Mohd Yusoff, M. Vasilopoulou, D. G. Georgiadou, L. C. Palilis, A. Abate, M. Khaja Nazeeruddin, *Energy Environ. Sci.* **2021**, *14*, 2906.
[22] G. Wu, R. Liang, M. Ge, G. Sun, Y. Zhang, G. Xing, *Adv. Mater.* **2021**, *33*, 202105635.
[23] S. Akin, B. Dong, L. Pfeifer, Y. Liu, M. Grätzel, A. Hagfeldt, *Adv. Sci.* **2021**, *8*, 2004593.
[24] M. Jung, T. J. Shin, J. Seo, G. Kim, S. I. Seok, *Energy Environ. Sci.* **2018**, *11*, 2188.
[25] J. J. Yoo, S. Wieghold, M. C. Sponseller, M. R. Chua, S. N. Bertram, N. T. P. Hartono, J. S. Tresback, E. C. Hansen, J.-P. Correa-Baena, V. Bulović, T. Buonassisi, S. S. Shin, M. G. Bawendi, *Energy Environ. Sci.* **2019**, *12*, 2192.
[26] S. Tan, T. Huang, I. Yavuz, R. Wang, T. W. Yoon, M. Xu, Q. Xing, K. Park, D.-K. Lee, C.-H. Chen, R. Zheng, T. Yoon, Y. Zhao, H.-C. Wang, D. Meng, J. Xue, Y. J. Song, X. Pan, N.-G. Park, J.-W. Lee, Y. Yang, *Nature* **2022**, *605*, 268.
[27] M. Pitaro, J. E. S. Alonso, L. D. Mario, D. G. Romero, K. Tran, J. Kardula, T. Zaharia, M. B. Johansson, E. M. J. Johansson, R. C. Chiechi, M. A. Loi, *Adv. Func. Mater.* **2023**, *31*, 2306571.
[28] M. Pitaro, J. S. Alonso, L. D. Mario, D. G. Romero, K. Tran, T. Zaharia, M. B. Johansson, E. M. J. Johansson, M. A. Loi, *J. Chem. Mater. A* **2023**, *11*, 11755.
[29] S. Kajal, J. Jeong, J. Seo, R. Anand, Y. Kim, B. Bhaskararao, C. Beom Park, J. Yeop, A. Hagdfeldt, J. Young Kim, K. S. Kim, *Chem. Eng. J.* **2023**, *451*, 138740.
[30] J. Suo, B. Yang, J. Jeong, T. Zhang, S. Olthof, F. Gao, M. Grätzel, G. Boschloo, A. Hagfeldt, *Nano Energy* **2022**, *94*, 106924.
[31] J. Li, L. Xu, T. Wang, J. Song, J. Chen, J. Xue, Y. Dong, B. Cai, Q. Shan, B. Han, H. Zeng, *Adv. Mater.* **2016**, *29*, 1603885.
[32] B. Yang, J. Suo, F. D. Giacomo, S. Olthof, D. Bogachuk, Y. Kim, X. Sun, L. Wagner, F. Fu, S. M. Zakeeruddin, A. Hinsch, M. Grätzel, A. D. Carlo, A. Hagfeldt, *ACS Energy Lett.* **2021**, *6*, 3916.
[33] J. Chen, J.-Y. Seo, N.-G. Park, *Adv. Energy Mater.* **2018**, *8*, 1702714.
[34] M. Wang, Y. Yin, W. Cai, J. Liu, Y. Han, Y. Feng, Q. Dong, Y. Wang, J. Bian, Y. Shi, *Adv. Funct. Mater.* **2022**, *32*, 2108567.
[35] M. V. Khenkin, E. A. Katz, A. Abate, G. Bardizza, J. J. Berry, C. Brabec, F. Brunetti, V. Bulović, Q. Burlingame, A. Di Carlo, R. Cheacharoen, Y.-B. Cheng, A. Colsmann, S. Cros, K. Domanski, M. Dusza, C. J. Fell, S. R. Forrest, Y. Galagan, D. Di Girolamo, M. Grätzel, A. Hagfeldt, E. von Hauff, H. Hoppe, J. Kettle, H. Köbler, M. S. Leite, S. (Frank) Liu, Y.-L. Loo, J. M. Luther, et al., *Nat. Energy* **2020**, *5*, 35.
[36] M. Kim, G.-H. Kim, T. K. Lee, I. W. Choi, H. W. Choi, Y. Jo, Y. J. Yoon, J. W. Kim, J. Lee, D. Huh, H. Lee, S. K. Kwak, J. Y. Kim, D. S. Kim, *Joule* **2019**, *3*, 2179.
[37] K. Karon, M. Lapkowski, *J. Solid State Electrochem.* **2015**, *19*, 2601.
[38] J. Xia, C. Liang, S. Mei, H. Gu, B. He, Z. Zhang, T. Liu, K. Wang, S. Wang, S. Chen, Y. Cai, G. Xing, *J. Mater. Chem. A* **2021**, *9*, 2919.
[39] A. A. Ashouri, A. Magomedov, M. Roß, M. Jošt, M. Talaikis, G. Chistiakova, T. Bertram, J. A. Márquez, E. Köhnen, E. Kasparavičius, S. Levcenco, L. G. Escrig, C. J. Hages, R. schlatmann, B. Rech, T. Malinauskas, T. Unold, C. A. Kaufmann, L. Korte, G. Niaura, V. Getautis, S. Albrecht, *Energy Environ. Sci.* **2019**, *12*, 3356.
[40] E. A. Alharbi, A. Krishna, N. Lempesis, M. Dankl, I. Mosquera-Lois, M. A. Hope, T. P. Baumeler, G. Kakavelakis, A. Mishra, F. T. Eickemeyer, O. Ouellette, T. Chawanpunyawat, A. Hagfeldt, S. M. Zakeeruddin, L. Emsley, L. Pfeifer, U. Roethlisberger, M. Grätzel, *Joule* **2023**, *7*, 183.
[41] H. Zhu, Y. Liu, F. T. Eickemeyer, L. Pan, D. Ren, M. A. Ruiz-Preciado, B. Carlsen, B. Yang, X. Dong, Z. Wang, H. Liu, S. Wang, S. M. Zakeeruddin, A. Hagfeldt, M. I. Dar, X. Li, M. Grätzel, *Adv. Mater.* **2020**, *32*, 1907757.
[42] R. T. Ross, *J. Chem. Phys.* **1967**, *46*, 4590.
[43] J. C. Garicía, E. R. Johnson, S. Keinan, R. Chaudret, J.-P. Piquemal, D. N. Beratan, W. Yang, *J. Chem. Theory Comput.* **2011**, *7*, 625.
[44] Y. Wang, T. Wu, J. Barbaud, W. Kong, D. Cui, H. Chen, X. Yang, L. Han, *Science* **2019**, *365*, 6454.